INTERNATIONAL JOURNAL of RENEWABLE ENERGY RESEARCH
C. V. Rodriguez et al., Vol.16, No.2, June, 2026

Methodology for Optimal Micrositing of Building Mounted Wind Turbines Using Computational Fluid Dynamics and Genetic Algorithms

Christian V. Rodriguez*‡, Alberto Ríos**, Jaime E. Luyo*

*Faculty of Mechanical Engineering, National University of Engineering, Lima, Peru

**Faculty of Systems, Electronics and Industrial Engineering, Technical University of Ambato, Ambato, Ecuador

(cvrodriguezd@uni.pe, a.rios@uta.edu.ec, jeluyo@yahoo.es)

‡Corresponding Author: Christian V. Rodriguez, Tel: +51 956 806671, cvrodriguezd@uni.pe

Received: 26.02.2024 Accepted: 14.04.2024

Abstract- Building Mounted Wind Turbines (BMWTs) are installed on building rooftops to exploit the wind velocity amplification found there. Optimal positioning of BMWTs (micrositing problem) can increase the energy gathered from the wind and reduce the total energy cost. Although micrositing methodologies have been extensively studied for wind farms, a gap in knowledge exists regarding the micrositing of BMWTs. The main objective of this work was to propose a methodology for optimal micrositing of BMWTs using Computational Fluid Dynamics (CFD) and Genetic Algorithms (GA). Thus, a site assessment was initially performed. Wind data treatment was carried out to determine those wind velocities and directions to be used in the next stages. These wind velocities and directions were simulated within an urban environment via CFD. The selection of a BMWT was then carried out. Furthermore, the zones with low wind speeds and high turbulence levels restricted the search space used in the GA-based micrositing optimization. Finally, a sensitivity analysis employing the building reinforcement factor (F) was performed. The results showed that the energy produced yearly by the BMWT is the key parameter in reducing the Cost of Energy (CoE), which achieved a value of 3.05146 $/kWh.

Keywords Micrositing, building mounted wind turbines, computational fluid dynamics, genetic algorithms.

1. Introduction

Greenhouse gas emissions produced by fossil fuel combustion are a concern for governments around the world. Over the last decades, this issue has been partially mitigated by substituting fossil fuels with renewable energies, which are essential for energy transition in many countries [1]. In the power generation sector, renewable energies such as hydro, solar and wind have been widely employed.

Wind energy is harvested by wind turbines, which can be classified by their size as small and large. Note that Small Wind Turbines (SWTs) have a rotor swept area smaller than 200 m2 [2]. Large wind turbines are typically installed in wind farms, while SWTs are commonly used in urban environments to partially supply residential and commercial loads [1]. SWTs can be Horizontal Axis Wind Turbines (HAWTs) or Vertical Axis Wind Turbines (VAWTs).

Regarding SWT design methodologies, the IEC 61400-2 methodology [2] comprises various test stages. Initially, the methodology defines operating parameters for SWTs. Subsequently, design methods for load analysis are applied, and electrical requirements are computed. Furthermore, environmental and mechanical tests are conducted, along with resonance and critical deflection analyses. Lastly, a support structure analysis is performed. Despite the multidisciplinary nature of the IEC 61400-2 methodology, some studies have criticized its applicability to SWTs installed in urban environments. For instance, Evans et al. [3] investigated the relationship between wind characteristics assumed in the IEC 61400-2 methodology and the performance of a 5 kW Aerogenesis turbine installed in two sites, Port Kennedy and Callaghan (Australia). The application of the IEC 61400-2 methodology revealed an underestimation of Turbulence Intensity (TI) for wind speeds (U) exceeding 4 m/s, a decrease in predicted mean power, and a reduction in damage

equivalent loading for the blade flapwise moment (< 58%). Consequently, the authors concluded that the IEC 61400-2 methodology is not suitable for SWTs installed in urban environments. Moreover, Rakib et al. [4] found high vertical wind speeds and significant fluctuations, with a standard deviation exceeding 2 m/s within an urban environment. Additionally, turbulence in vertical velocities was found to be 20% higher than those indicated in the IEC 61400-2 methodology, revealing its inadequacy for SWTs.

Within urban environments, SWTs can be installed on building rooftops, i.e., Building Mounted Wind Turbines (BMWTs), to exploit the wind velocity amplification found in such location. It's worth noting that the building serves as a tall tower for the turbine, allowing it to gain height and thereby increase its power output.

Knowledge of urban wind behavior is essential for the proper design and installation of BMWTs. However, predicting urban wind patterns through on-site measurements is challenging. To address this issue, designers have employed a Computational Fluid Dynamics (CFD) approach to predict wind flow behavior and enhance the efficiency of wind turbines in the past [5]. This approach is also employed in the present work.

Heath et al. [6] conducted a study on wind flow behavior in an urban environment consisting of 24 houses using CFD. The authors observed wind energy with changing wind directions and provided insights into the optimal locations for placing wind turbines on the rooftops of houses. Similarly, Tabrizi et al. [7] utilized CFD to simulate a real urban environment located in Australia. The CFD results exhibited good agreement with wind velocity measurements, with a maximum error of 30.3% observed for the North-East direction. The authors concluded that the center of the building rooftop was the most suitable location for installing a HAWT, as it would experience fewer fatigue loads due to vertical flow. Moreover, Juan et al. [8] performed a numerical study to assess the urban wind energy potential around high-rise buildings in a highly urbanized area. The CFD results were compared to wind measurements, with a maximum deviation of 20% for U, wind direction and TI. The authors concluded that upstream obstacles decrease wind power and increase turbulence levels downstream.

Evaluation methodologies for BMWTs have been also conducted in the past. Gagliano et al. [9] proposed a methodology that utilized CFD simulations and databases integrated into a geographical information system to assess the feasibility of BMWTs. A case study was conducted, being an urban area in San Cataldo (Italy), where three types of BMWTs were tested: a HAWT and two VAWTs (Darrieus and Savonius). Wind direction effects were investigated through simulation of four wind directions. The authors concluded that the Darrieus VAWT produced 61.32% more energy than the HAWT. Deltenre and Runacres [10] performed a feasibility study for instaling a 3 kW HAWT on a 150 m tall building called South Tower (Belgium). Their methodology comprised micrositing, stability assessment, environmental concerns evaluation, and economic analysis. The environmental concerns included noise, shadow flicker, visual impact, biodiversity, and air traffic analyses. The optimal location for the turbine was determined to be on the upstream side of the building rooftop. The economic viability analysis revealed a high study cost, with a levelized cost of energy ranging between 0.95 and 0.36 €/kWh for mean wind velocities between 4 and 6 m/s, respectively. Additionally, Arteaga-López et al. [1] developed a methodology for assessing the installation of BMWTs using CFD simulations. They applied this methodology to a case study involving the installation of 5 BMWTs on a university building rooftop in Mexico, capable of generating 104 802 kWh yearly. However, the study only considered one wind direction and velocity. The authors concluded that their methodology could reduce time and costs of feasibility studies for wind projects. Similarly, Shiraz et al. [11] developed a methodology for assessing the performance and power output of BMWTs, combining CFD simulations with meteorological data. They conducted simulations for two sites in Montreal (Canada), representing downtown and commercial areas. Wind velocities were estimated at four control points, representing BMWTs positions, for wind from eight different directions. Annual energy outputs between 15 and 408 kWh were estimated for a Darrieus turbine located at the control points. The authors suggested that their methodology could analyze multiple sites and turbines simultaneously. Despite the advancements noted in these works, optimal micrositing of BMWTs, which could enhance their power outputs and reduce wind projects costs, was not considered.

Various studies related to micrositing optimization have been applied to wind farms, representing one of the most important technologies used to enhance wind power utilization [12]. In this sense, Moorthy et al. [13] proposed a novel approach for optimizing the placement of wind turbines in a wind farm to maximize power output using Genetic Algorithms (GA). Their methodology offered greater flexibility compared to other works because the search space did not rely on square grids to divide the plot. They employed Jensen's wake model to represent the momentum conservation in the wake downstream of the wind turbine. The authors used a population size of 600 individuals for the GA. Additionally, Moorthy et al. [14] proposed another approach for determining the optimal placement of wind turbines in a wind farm to maximize power output, using particle swarm optimization. They also utilized the wake model and compared their approach with past methods in the literature that focused on optimizing wind turbine placement, primarily using GA. Rajper and Amin [15] investigated the micrositing problem applied to a wind farm, considering a fixed hub height and employing GA to minimize the cost per unit power. Their study resulted in a final layout comprising 54 wind turbines, achieving an overall efficiency of 97% and a non-dimensionalized cost per unit power of 1.3292x10-3. Micrositing of wind farms often employs the linear wake model, developed by Jensen, to quantify the reduction in wind velocities behind large wind turbines. Chen et al. [12] studied wind turbine layout optimization using two hub heights and the Greedy algorithm to minimize the cost per unit power output. They utilized both the linear wake model and the particle wake model for wake flow predictions over flat and complex terrains, respectively. Their findings indicated that the layout with two hub heights significantly increased total

power output and reduced the cost per unit power output to 1.046 €/W for U = 14 m/s compared to layouts with only one hub height. Similarly, Song et al. [16] studied wind turbine layout optimization with multiple hub heights on flat terrain, employing the Gaussian particle swarm algorithm to minimize the cost per unit power output ratio. Their numerical results showed the necessity of three-dimensional optimization to address the micrositing problem effectively. Furthermore, Hu et al. [17] proposed an approach for wind farm micrositting in complex terrain using meteorological measurements, CFD and GA. Their approach incorporated a variable mutation rate to avoid GA find local optimum. Compared to the Greedy algorithm, GA exhibited relatively better results in terms of probability of finding the global optimum, achieving an objective function (OF) 5.2% lower than the Greedy algorithm. For this reason, GA are utilized in the present work.

It is important to note that Ovgor et al. [18] proposed a method for the optimal micrositing of BMWTs using Weibull distribution and CFD. Their study utilized wind data comprising 52 505 measurements performed between May 2008 and May 2009. The data were grouped into bins of 1 m/s for velocities and 16 wind directions. Simulating a cubed-shaped building model with a side length of 50 m, the authors estimated wind flow acceleration on the building rooftop across 9 positions at 3 m above the rooftop. The CFD simulations employed the CFX solver to solve the Unsteady Reynolds-Averaged Navier Stokes (URANS) equations, with a mesh containing 5'800 000 tetrahedral cells. Using the Aeronet AN-TR2 VAWT of 2 kW, the authors calculated the energy generated via the turbine power curve, achieving annual values ranging from 0 to 1 444 kWh for the 9 positions. The optimal position was determined based on the highest energy generated and the dominant wind direction. Similarly, Wang et al. [19] conducted a micrositing study to identify the best locations for BMWTs over the Engineering and Technology Building (Building A), employing CFD simulations and lidar measurements. Their micrositing method included both preliminary and accurate stages. Preliminary micrositing simulated only the main wind direction, while accurate micrositing considered 8 wind directions. The results indicated that the optimal location for installing BMWTs was near the upstream side of the building at heights ranging from 1.51 to 1.79 times the building height, where wind acceleration reached its maximum value. However, this study did not perform an optimization, which could potentially reduce the energy costs of the BMWTs, as seen in wind farms. Arteaga-López and Angeles-Camacho [20] also developed a methodology for wind energy assessment and micrositing of BMWTs. Their methodology utilized a triacontakaihexagonal prism geometry as computational domain, allowing simulation of 36 multidirectional flows obtained from a wind rose. The results demonstrated that the methodology could facilitate the micrositing of four BMWTs.

Accordingly, the main objective of this work is to propose a methodology for the optimal micrositing of BMWTs using CFD simulations and GA. Firstly, a site assessment is performed, and recommendations regarding installation feasibility are provided. Next, wind data are processed to determine the velocities and directions to be utilized in subsequent stages. These wind velocities and directions are then simulated within an urban environment via CFD (wind resource assessment stage). Based on the CFD results, a BMWT is selected, and its power curve is obtained through CFD simulations. Two numerical models, one representing the building and the other representing the wind turbine, must be validated to ensure the reliability of the numerical results. Furthermore, restrictions concerning zones with low wind velocities and high wind turbulence levels are identified. These restrictions are incorporated into the micrositing optimization process to determine the optimal solution, i.e., the optimal position for the BMWT on the building rooftop, aiming to minimize the Cost of Energy (CoE). It is important to note that the installation cost is estimated using a simplified cost model, while the energy produced is calculated based on the wind velocities, obtained from the wind resource assessment stage, and the wind turbine power curve.

The proposed methodology is outlined in Section 2, while Section 3 presents the results of this study. Finally, Section 4 concludes the findings.

2. Methodology

The methodology proposed is depicted in Figure 1, and each stage is described in the following subsections. The methodology begins with a site assessment stage, where the search space to position the BMWT is chosen based on normative restrictions. Next, wind data is analyzed statistically to determine which wind velocities and directions will be used in the wind resource assessment stage. This last stage serves to find the velocity distribution above the target building rooftop (first generated database), simulating the urban environment of interest where the BMWT will be installed. In the wind turbine design stage, the characteristics of a previously chosen wind turbine model (power curve) can be determined. This power curve represents a second generated database. To ensure feasible results, both models for the urban environment and wind turbine, are validated by comparing them with experimental measurements. It's important to note that the wind resource assessment, wind turbine design, and model validation stages involve CFD simulations. Finally, a micrositing optimization is performed to determine the best position to install the wind turbine above the target building rooftop. The optimization is carried out using GA and the databases mentioned earlier.

2.1. Site Assessment

This stage comprises preliminary analyses required to assess the feasibility of installing BMWTs in specific areas. It involves understanding the laws and regulations governing the site where the BMWT will be installed. Analyses concerning building structure restrictions are crucial, determining whether it is feasible to install BMWTs and if the structure can support the turbine without requiring building structure reinforcement [21]. Moreover, considerations such as space limitations on building rooftops, environmental concerns, noise regulations, and potential social resistance should also be taken into account in the analyses. Once these restrictions are addressed, subsequent stages of the proposed methodology can proceed.

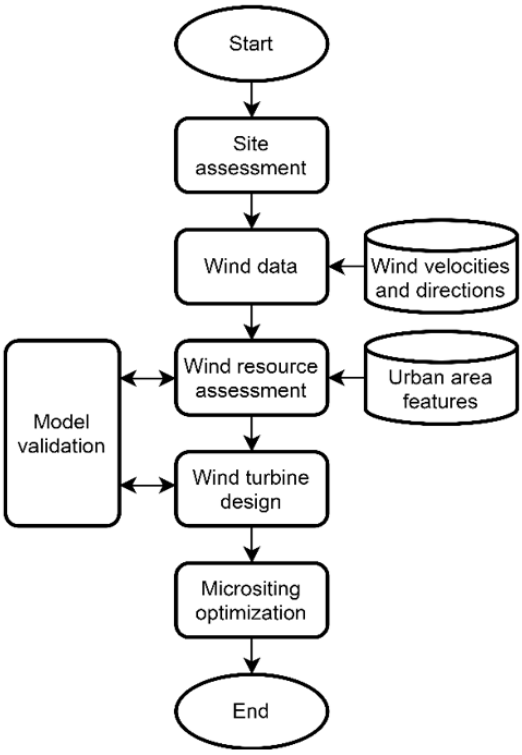

Fig. 1. Methodology proposed.

2.2. Wind Data

Wind measurements are typically conducted by institutes, universities and meteorological centers near the urban area to be modeled. Conventional techniques for measuring wind characteristics involve collecting data for up to a year [6].

In this work, the wind data treatment is performed using a wind rose code implemented in Python [22]. The wind rose is organized into 16 directions, with velocity bins of 1 m/s width. The average velocity per bin (U_{avg}) is computed from the cubic values of wind velocities, which represent the available wind energy that wind turbines can exploit. The formulation of U_{avg} is, as follows,

$$U_{avg} = \sqrt[3]{\frac{\sum_{i=1}^{n} U_i^3}{n_j}}, \quad (1)$$

where U_i and n_j represent the wind velocities and the number of velocity measurements per bin, respectively.

Furthermore, a table showing occurrence frequency of velocities and directions is constructed. The average velocities and directions that represent the highest occurrences will be used in the subsequent CFD simulations stages. It is crucial to discard velocities and directions with low level of occurrence to minimize the number of CFD simulations.

2.3. Model Validation

The model validation stage comprises mesh independence studies, where a comparison between numerical results and experimental measurements is conducted. This study aids designers in understanding the level of accuracy of the numerical models.

The results of two numerical models, a building and a wind turbine, are validated in this work. The building model is utilized in the wind resource assessment stage, while the wind turbine model is employed in the wind turbine design stage. The results obtained in these stages are utilized in the micrositing optimization process.

The Reynolds-Averaged Navier Stokes (RANS) approach is widely utilized for engineering applications due to its lower computational cost compared to Large Eddy Simulation (LES) and Direct Numerical Simulation (DNS) methods. It's worth noting that while RANS is less accurate than LES and DNS, it has been selected for this work. Additionally, steady-state simulations are adopted here because they require fewer computational resources than unsteady simulations. The RANS formulation for steady-state, incompressible flow of Newtonian fluid can be written,

$$\frac{\partial \bar{u}_i}{\partial x_i} = 0, \quad (2)$$

$$\frac{\partial (\bar{u}_i \bar{u}_j)}{\partial x_j} = -\frac{1}{\rho}\frac{\partial \bar{p}}{\partial x_i} + \frac{\partial}{\partial x_j}\left(\nu \frac{\partial \bar{u}_i}{\partial x_j} - \overline{u_i' u_j'}\right), \quad (3)$$

for the mass and momentum conservation, respectively. The Realizable k-ε and SST k-ω turbulence models are used here to treat the Reynolds stress $\overline{u_i' u_j'}$ of the RANS formulation, for the building and wind turbine simulations, respectively. These turbulence models have been chosen because they have demonstrated an acceptable trade-off between accuracy and computational cost in simulations of the building and wind turbine in a prior study [23].

ICEM CFD and Fluent are utilized to construct the meshes and conduct the CFD simulations, respectively. The simulations are executed on a computer equipped with 16 cores and 64 GB of RAM memory, utilizing 12 cores in parallel. The SIMPLE algorithm is employed, and the least squares cell-based method is used for gradients. Second-order schemes are utilized for pressure, momentum, k, ε and ω. The convergence criterion is set with residuals of 10^{-5} for all variables. **Table 1** presents the general parameters used in the CFD simulations.

Table 1. General simulation parameters

Parameter	Value
State	Steady
Mesher	ICEM CFD
Solver	Fluent
Algorithm	SIMPLE
Gradients	Least squares cell-based
Schemes	Second-order
Residuals	10^{-5}

2.3.1. Building

A computational domain comprising a building of 15.24 m (width) x 15.24 m (length) x 30.48 m (building height, H) is simulated. The computational domain is a hexadecagon with an edge length of 194 m and a total height of 342.9 m (see Figure 2). The Ground (bottom) and Building surfaces are

designated as walls, while the Sky boundary (top) is treated as symmetry plane. Specifically, 7 surfaces from the outer domain are treated as velocity-inlet boundaries, 7 surfaces are set up as pressure-outlet boundary conditions, and 2 surfaces are symmetry planes. For example, when the wind blows from S to N, the surfaces WSW, SW, SSW, S, SSE, SE and ESE are velocity-inlet boundaries, WNW, NW, NNW, N, NNE, NE and ENE are pressure-outlet boundaries, and W and E are symmetry planes. The inlet surfaces are set up with an atmospheric boundary layer determined by the power law as,

$$u_z = u_r \left(\frac{h_z}{h_r}\right)^{\alpha}, \quad (4)$$

where u_z is the velocity extrapolated at the height h_z, u_r represents the velocity measured at the reference height h_r, and α is the Hellman coefficient.

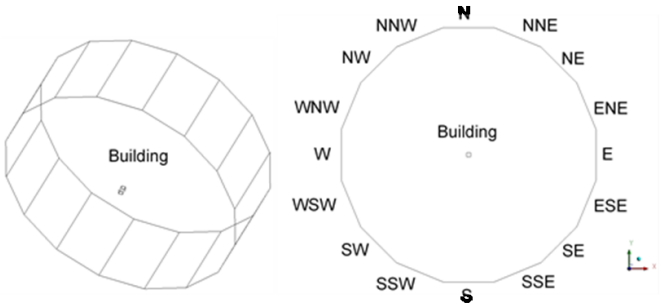

Fig. 2. Computational domain of the building.

Three meshes (Coarse, Medium and Fine) are tested in the mesh independence study, containing 3'948 800, 8'101 184 and 16'786 752 cells, respectively. On all walls, y+ < 5 are kept, with values within the acceptable range for employing the Realizable k-ε turbulence model [24] with enhanced wall treatment. It is important to note that the results of U and turbulent kinetic energy (k), only evaluated at the middle position above the building rooftop, are compared, since the focus of the present work is primarily on airflow interaction with the wind turbine located above the rooftop. A validation process of the building is not conducted here, as there is no experimental data for the model. Table 2 shows the CFD parameters employed for simulating the building.

2.3.2. Wind turbine

The validation of the wind turbine CFD results was conducted in a previous study [23]. The numerical model corresponded to the MEXICO wind turbine [25], which features three blades and a rotor diameter of 4.5 m. The blades are composed of DU 91-W2-250, RISØ A1-21 and NACA 64-418 airfoils. Note that the hub, nacelle and tower were not considered in the CFD simulations (see Figure 3). The simulations were performed using the SST k-ω turbulence model [26]. As seen in Figure 3, the simulations comprised two domains (stationary and rotational). The Front and Back surfaces were set up as periodic, while the top and bottom faces were treated as symmetry and slip conditions, respectively. The Inlet surface was imposed with different wind velocities, and Outlet was set up with gauge pressure. In [23], four meshes, Coarse, Medium, Fine and Extra Fine, containing 5'149 318, 8'094 168, 14'932 927 and 24'703 452 cells, respectively, were employed in the simulations. Table 3 depicts the CFD parameters utilized for simulating the wind turbine.

Table 2. CFD parameters for the building

Parameter	Value
Turbulence model	Realizable k-ε
Domain geometry	Hexadecagon
Domain size	Edge length = 194 m Total height = 342.9 m
Building size	15.24 m (width) 15.24 m (length) 30.48 m (height)
Boundary condition	Ground (wall) Building surfaces (wall) Sky (symmetry) 7 outer surfaces (velocity-inlet) 7 outer surfaces (pressure-outlet) 2 outer surfaces (symmetry)
Inlet velocity	Velocity profile computed using Equation (4)

Table 3. CFD parameters for the wind turbine [23]

Parameter	Value
Turbulence model	SST k-ω
Domain geometry	Cylindrical 1/3
Domain size	Stationary internal radius = 2.7 m Rotational external radius = 11.3 m Domain length = 24.75 m
Wind turbine size	Rotor diameter = 4.5 m DU 91-W2-250, RISØ A1-21 and NACA 64-418 airfoils
Boundary condition	Turbine (wall) Top (symmetry) Outlet (pressure outlet) Inlet (velocity inlet) Front and Back (periodic) Bottom (slip)
Inlet velocity	10 m/s

2.4. Wind Resource Assessment

The effective operation of wind turbines depends not only on site selection, but also on accurate wind resource assessment [28]. In this stage, it is crucial to identify the target building where the BMWT will be installed and to assess the surroundings that could influence wind flow behavior within the urban environment.

To determine the optimal location for installing the BMWT, it is recommended to simulate all wind velocities and directions present in the urban area under study. Indeed, this approach differs from conventional CFD studies where analysis is typically focused only on the prevailing wind velocity and direction [20]. Based on characteristics of each site, it is possible to avoid simulations of specific wind conditions, which is the approach adopted in the present work. Representative wind velocities and directions should be

simulated at least, especially when it is not possible to analyze all cases due to limited computational resources.

After the simulations are performed, comprehensive analyses of wind flow above the target building rooftop will be carried out to identify zones where wind velocity amplification and low turbulence levels occur, as indicated by the check mark in Figure 4. These zones will define potential positions, above the building rooftop, where BMWTs can be installed, i.e., the search space for the micrositing optimization.

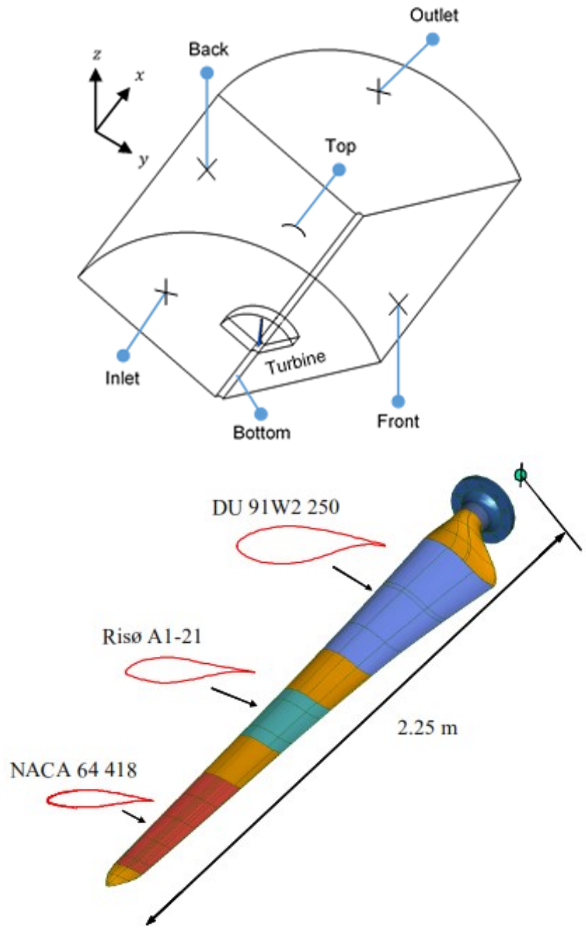

Fig. 3. Domain geometry [23] and MEXICO wind turbine blade [27].

2.5. Wind Turbine Design

Based on the electrical energy consumption of the target building, the power output of the BMWT can be estimated. This power output will be used to design or choose an appropriate wind turbine rotor topology. Designing the rotor geometry of the BMWT can be accomplished using procedures based on the Blade Element Momentum (BEM) theory, as outlined by Manwell et al. [29]. Alternatively, the selection of commercial wind turbines can be made by employing manufacturer's datasheets, which contain information about power curves.

In addition to technical norms and regulations specific to each site, region or country, the type and size of BMWTs may be further constrained. These restrictions could pertain to power output, noise levels, vibration levels and the flicker effect generated by wind turbines. The implementation of these additional restrictions can be considered as part of future work. Moreover, it is highly advisable to conduct mechanical analyses of BMWTs. This is particularly important because commercial turbines designed under the IEC methodology may not guarantee acceptable levels of reliability and safety, as mentioned in [3][4]. This aspect can also be considered as part of future work.

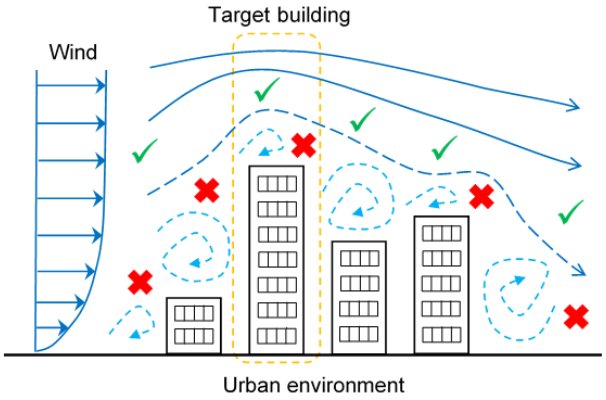

Fig. 4. Airflow behavior in an urban environment.

2.6. Micrositing Optimization

The higher the turbine rotor is placed, the installation costs increase due to the requirement for a larger tower. However, higher placement also exposes the turbine to greater wind speeds, which can be harvested by the BMWT, as depicted in Figure 5. In practice, the rotor height is empirically determined, as turbulence levels and wind directions on the building rooftop are not definitely known. Therefore, it cannot be guaranteed that the BMWT will capture sufficient wind energy to generate the required quantity of electricity for the user.

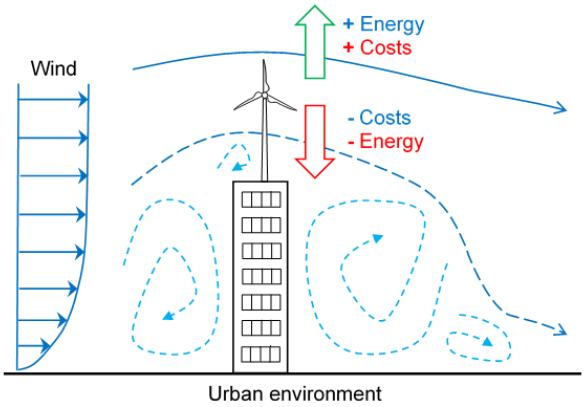

Fig. 5. Wind turbine rotor positioning on the building rooftop.

To address the unpredictability of wind directions, CFD simulations of wind flow passing through an urban environment can be conducted to understand the associated phenomenology. Additionally, the issue of low wind speeds can be partially mitigated by positioning the BMWT rotor at higher altitudes. As a result, optimal micrositing of the BMWT rotor can be achieved, ensuring that the wind flow

entering the turbine maintains low turbulence levels and high wind speeds. This maximizes energy capture from the wind (total energy generated) while minimizing rotor height to avoid incurring high installation costs for the BMWT. Note that determining how new BMWT designs can impact performance and system costs is critical [30].

As explained in the introduction section, most micrositing studies aim to minimize the cost per unit power of wind turbines installed in wind farms. It is important to note that the costs associated with wind farms can be estimated using a cost breakdown scheme developed by NREL [30]. However, a similar cost breakdown scheme for BMWT costs has not been established yet [31], mainly due to limited empirical data on distributed wind projects [32]. Hence, it is necessary to propose a simplified cost model for BMWTs. In this work, a cost model similar to those found in [12] and [16] is employed, which comprises a base cost (C_b) and a cost per height (C_z). Based on a 10 kW residential wind turbine with a 31 m guyed tower [33], the tower accounts for 20% ($ 14 145) of the total wind turbine cost ($ 68 195). Moreover, SWTs have total installation costs of 6 000 $/kW for power outputs between 11 and 100 kW [34]. For the MEXICO wind turbine, with 15 kW power output at 15 m/s [25], the cost parameters are determined as C_b = $ 72 000 and C_z = 456.29 $/m. These costs are then divided by the total energy produced by the turbine over a period of 20 years (CoE) to define the objective of the optimization process (OF), as follows,

$$OF = \frac{456.29\,z+72\,000}{Energy}. \quad (5)$$

The OF will be minimized by modifying the wind turbine hub height (z) and its projection on the building rooftop (x and y), as illustrated in Figure 6. It's worth noting that the wind turbine rotor size remains constant throughout the optimization process.

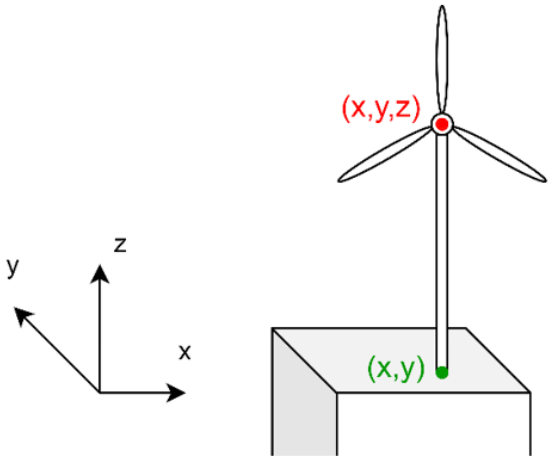

Fig. 6. Arrangement for optimization.

The optimization is conducted using GA implemented in MATLAB. GA is an efficient search method originally proposed by J.H. Holland, which is based on the principles of evolution and natural selection theory [35]. GA involves various key elements, including chromosome representation, fitness selection, and biological-inspired operators [36] [37]. These operators include selection, mutation, and crossover, and their ratios are challenging to estimate accurately [35].

The selection of population size is a critical factor in balancing between premature convergence to local optimal solutions and computational effort required to achieve the global optimal solution [38]. In the present work, a population size of 30 individuals is utilized, which is determined by multiplying 10 by the number of variables, which is a conservative approach. The tournament selection technique is employed due to its efficiency [39], with a tournament size of 2 to preserve diversity [37]. Additionally, the elitism operator is selected to retain the best individual across generations. For crossover, the heuristic crossover method is utilized, which returns a child positioned on the line containing the two parents, a small distance away from the parent with better fitness. The crossover fraction is set to 0.8. The mutation function selected is mutation adapt feasible, which chooses a direction and step length that satisfy bounds and linear constraints. These parameters are depicted in Table 4.

Table 4. GA parameters

Parameter	Value
Population size	30
Selection function	Tournament
Tournament size	2
Elite count	1
Crossover function	Heuristic
Crossover fraction	0.8
Mutation function	Adapt feasible

The convergence criteria of the optimization process [40] are as follows,

$$\frac{\max(OF_i)-\max(OF_{i-1})}{\max(OF_i)} < 10^{-3}, \quad (6)$$

$$\frac{\text{std}(OF_i)}{\max(OF_i)} < 10^{-3}, \quad (7)$$

where i indicates the generation of the optimization process.

Additionally, a sensitivity analysis is conducted by varying C_z. It is assumed that C_z can increase by a factor (building reinforcement factor, F) if an additional building structure is required to support the BMWT. Consequently, the CoE formulation will be adjusted for the sensitivity analysis as follows,

$$CoE = \frac{456.29\,F\,z+72\,000}{Energy}, \quad (8)$$

where F will take values of 1, 5, 10, 15, 20 and 25.

3. Results and Discussion

A single hypothetical building located in the Jesus Maria district (Lima, Peru) is studied in this work. Using only one building (target building) to represent the urban environment is acceptable when surrounding structures, such as other buildings, are low-rise, which is the assumption made here.

3.1. Site Assessment

It is assumed that there is only one restriction for the installation of BMWTs at the site studied, which is related to the visual impact caused by the rotation of wind turbines blades on humans. To address this issue, the available space (S_i) for installing the wind turbine rotor must be restricted, as illustrated in Figure 7. The lower bound of the available space depends on low wind velocities and high turbulence zones that need to be avoided, while the upper bound is restricted by a maximum height equal to the building height above the rooftop.

Alternatively, the available space can be further restricted by people's visual fields (alternative space), which are located at a distance of 14 m (w_s) from the building base, projected onto the building rooftop (see Figure 8). This distance can be considered as the typical street width in the Jesus Maria district. Note that the visual fields are projected above the building rooftop, taking into account people of average height (1.65 m). This alternative space consideration could be explored in future works.

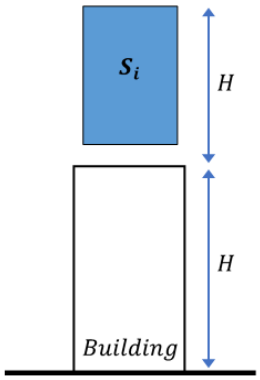

Fig. 7. Available space for installing the wind turbine rotor.

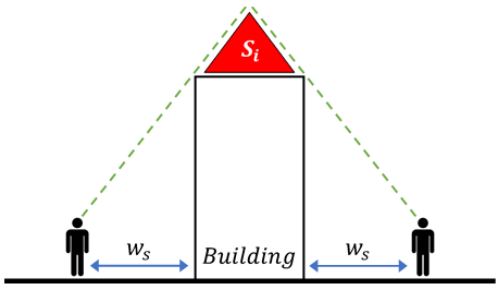

Fig. 8. Alternative space for installing wind turbine rotors.

3.2. Wind Data

The wind data used in this study consists of measurements of wind velocities and directions performed collected at a height of 10 meters above the ground level at Campo de Marte station in the Jesus Maria district, conducted by Servicio Nacional de Meteorología e Hidrología (SENAMHI). These measurements were taken hourly throughout the year from January 1st to December 31st, 2020. In total, there were 8 643 wind measurements used here, consisting of 8 643 velocity readings and 8 643 direction readings, with 117 measurements excluded due to missing data.

Figure 9 illustrates the daily average wind velocities, revealing that the majority of daily averages fall within the range of 1.5 and 3 m/s. The yearly average wind velocity was 2.3 m/s.

Using the previously mentioned wind velocities and directions, a wind rose is constructed as depicted in Figure 10. The color bars represent wind velocity bins as indicated in the legend, while the concentric circles indicate the probability of velocities occurring within each bin.

As seen in Figure 10, velocities have predominantly occurred in the SSW and SW directions, accounting for 81.8% of occurrences. Additionally, wind velocities between the S and W directions represent 94.7% of the total occurrences, as shown in Table 5. This table also presents the U_{avg} values calculated using Equation (1).

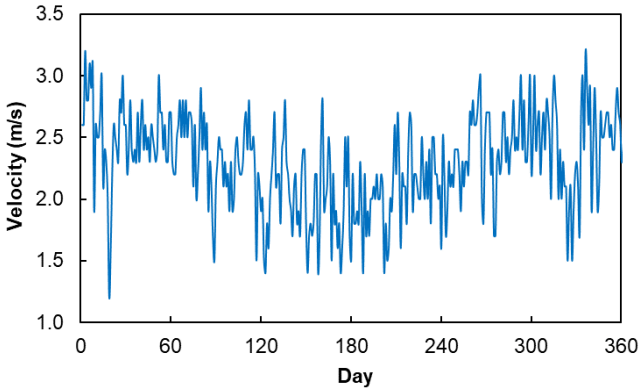

Fig. 9. Daily average wind velocities.

Since most wind turbines have a cut-in speed above 3 m/s, it is unnecessary to simulate wind conditions below this threshold. By using Equation (4), wind velocities of 2.18 and 3.41 m/s, calculated at H, are determined from U_{avg} values of 1.56 and 2.44 m/s, respectively, considering $\alpha = 0.3$ and $h_z = 30.48$. Thus, this study only considers $U_{avg} \geq 2.44$ m/s, which are highlighted in a green box in Table 5. Moreover, CFD simulations are conducted for five wind directions (highlighted in a cyan box) to assess wind energy potential on the building rooftop. Therefore, a total of 20 cases (highlighted in a red box, Table 5) are analyzed in the wind resource assessment stage, but only 15 cases are simulated using wind directions S, SSW and SW. Note that the WSW and W directions are treated similarly to SSW and S, respectively, due to the symmetry of the building's topology.

3.3. Model Validation

3.3.1. Building

To establish the velocity profile for the Inlet surfaces of the computational domain, a wind velocity of 7.2 m/s is prescribed at a height of 10 m (h_r), computed using Equation (4). These simulations employ the Realizable k-ε turbulence model with enhanced wall treatment, considering $\alpha = 0.30$, which is a conservative value for urban areas. Figure 11 illustrates the results for U and k obtained using three different meshes at the middle line above the building rooftop.

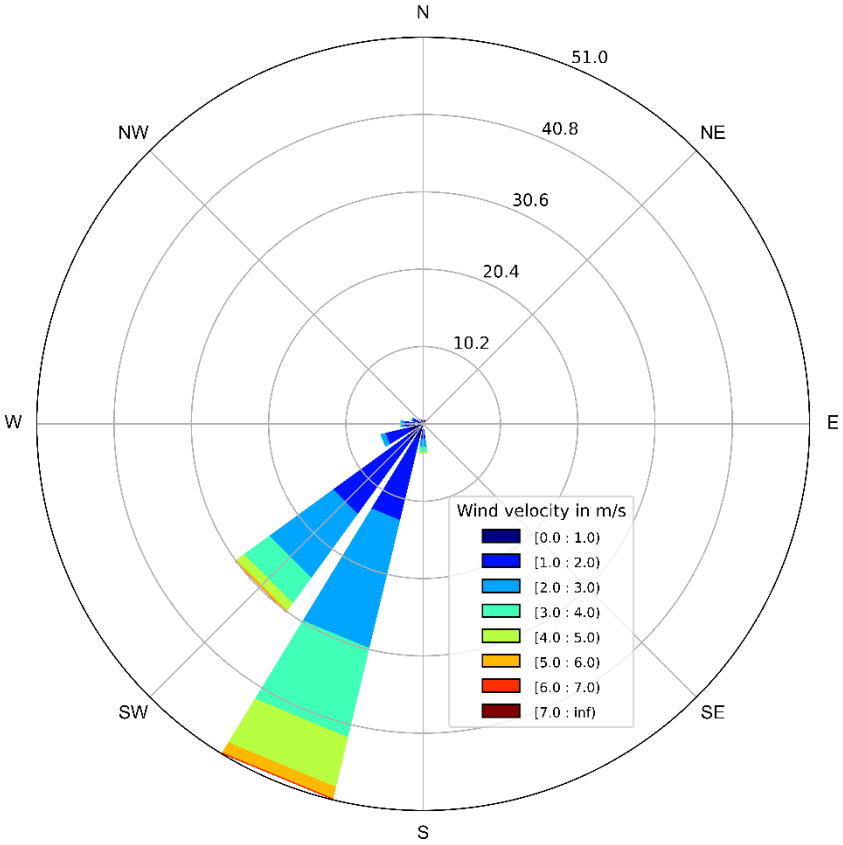

Fig. 10. Wind rose based on wind data from Campo de Marte station.

Table 5. Occurrence of wind velocities (%)

Interval (m/s)	U_{avg} (m/s)	N	NNE	NE	ENE	E	ESE	SE	SSE
[0 - 1>	0.64	0.59	0.57	0.36	0.13	0.09	0.06	0.09	0.08
[1 - 2>	1.56	0.03	0.03	0.06	0	0	0	0.01	0.02
[2 - 3>	2.44	0	0	0	0	0	0	0	0
[3 - 4>	3.43	0	0	0	0	0	0	0	0
[4 - 5>	4.38	0	0	0	0	0	0	0	0
[5 - 6>	5.30	0	0	0	0	0	0	0	0
[6 - 7>	6.23	0	0	0	0	0	0	0	0
[7 - 7.4]	7.21	0	0	0	0	0	0	0	0
Total		0.62	0.60	0.42	0.13	0.09	0.06	0.10	0.10
Interval (m/s)	U_{avg} (m/s)	S	SSW	SW	WSW	W	WNW	NW	NNW
[0 - 1>	0.64	0.59	1.93	2.55	2.00	1.49	0.89	0.74	0.59
[1 - 2>	1.56	1.39	11.13	12.13	3.12	0.97	0.57	0.10	0.07
[2 - 3>	2.44	1.10	17.37	10.46	0.69	0.46	0.19	0.02	0
[3 - 4>	3.43	0.67	12.08	4.11	0.06	0.13	0.03	0	0
[4 - 5>	4.38	0.16	6.76	1.27	0	0.01	0	0	0
[5 - 6>	5.30	0.01	1.56	0.23	0	0	0	0	0
[6 - 7>	6.23	0	0.17	0.03	0	0	0	0	0
[7 - 7.4]	7.21	0	0.02	0	0	0	0	0	0
Total		3.92	51.02	30.78	5.88	3.07	1.68	0.87	0.66

The deviation between the Medium and Fine meshes is relatively low for U, with a maximum value of 1.35% (Figure 11a). Similarly, the results for k obtained with these meshes are closely similar (Figure 11b). Due to negligible discrepancies observed in results for U and k between the Medium and Fine meshes, the Medium mesh is selected for subsequent CFD simulations.

The Medium mesh details are depicted in Figure 12. The height of the first cell adjacent to the building surfaces and the Ground is $1x10^{-6}$ and $2x10^{-6}$ m, respectively, ensuring that y+ remains below 5 on all walls. Coarser elements are positioned farther from the building location, while finer elements are concentrated around the building surfaces where high flow gradients occur, as shown in Figure 12a. Similarly, finer elements are placed near the edges of the building, as illustrated in Figures 12b and 12c. Note that the building comprises 104 edge cells and 106 height cells.

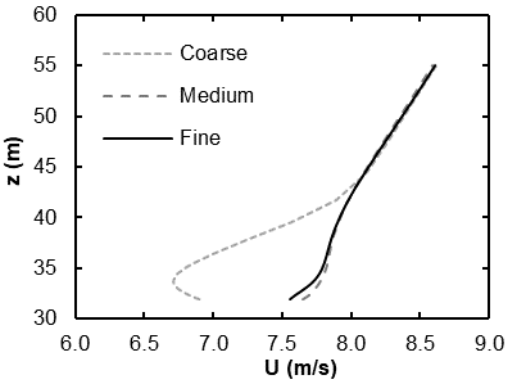

(a)

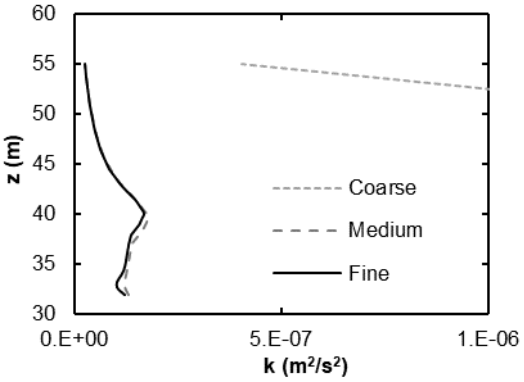

(b)

Fig. 11. Vertical profiles of U (a) and k (b) on the middle line above the building rooftop. Mesh independence study.

3.3.2. Wind turbine

In the validation of the wind turbine results, a grid independence study was conducted using the SST k-ω turbulence model. In this validation, numerical results obtained with four different meshes were compared with thrust and torque measurements. The validation was performed in a previous study [23] for U = 10 m/s, which is higher than the velocities used in this work. Hence, acceptable results are expected when using velocities determined in the wind data stage (section 3.2). Table 6 summarizes the results of the validation. Based on the results, it was concluded that grid independence is achieved with the Medium mesh, as the errors between the Medium and Fine meshes are lower than 0.8% and 2.2% for thrust and torque, respectively. Therefore, the Medium mesh will be utilized in the subsequent CFD simulations.

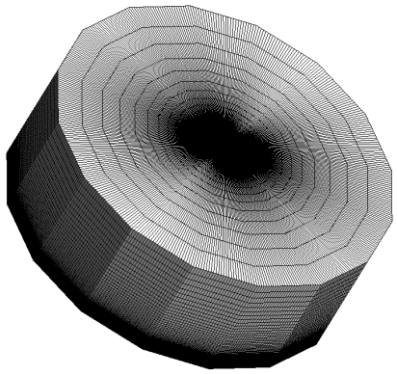

(a)

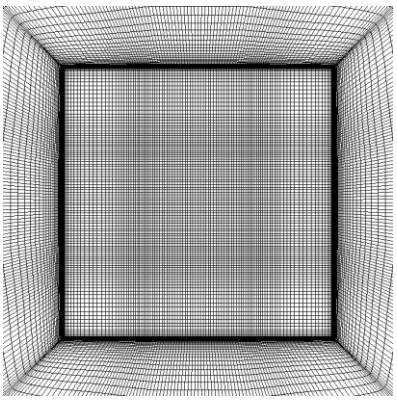

(b)

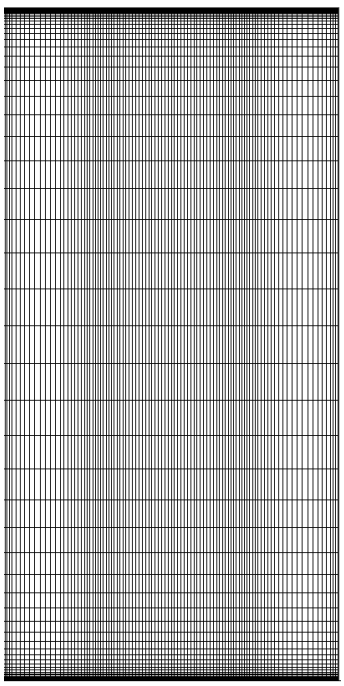

(c)

Fig. 12. Details of the Medium mesh. External domain (a), top view (b) and elevation view (c) of the building.

Table 6. Numerical thrust and torque obtained for U = 10 m/s. Grid independence study [23]

Mesh	Thrust (N)	Torque (N m)
Coarse	964.083	37.259
Medium	1135.539	86.507
Fine	1127.493	84.625
Extra Fine	1124.889	83.904

The details of the Medium mesh are shown in Figure 13. Notably, a large number of cells is are concentrated near the leading and trailing edges of the profiles, anticipating higher gradients of flow parameters in these regions. The first cell height on the blade surfaces is 10^{-6} m.

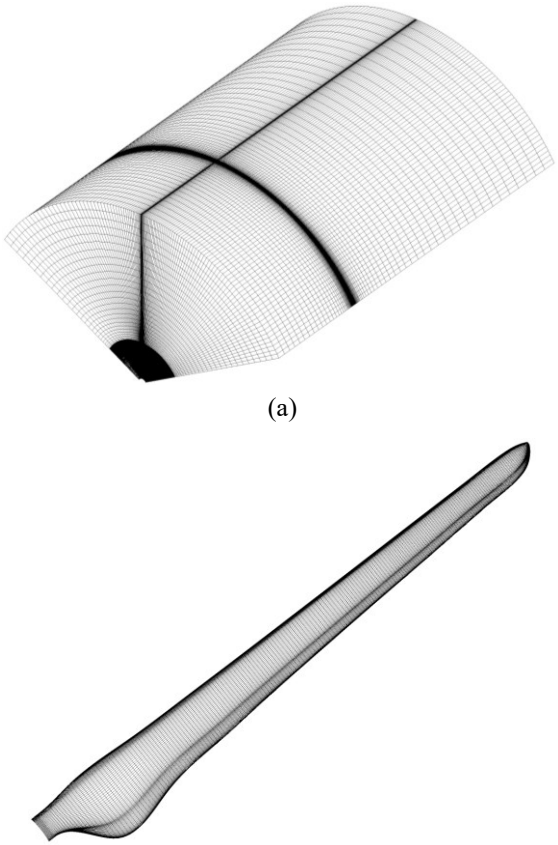

(a)

(b)

Fig. 13. Details of the Medium mesh [23]. External domain (a) and wind turbine blade (b).

3.4. Wind Resource Assessment

Using the validated building model, 15 cases are simulated to assess the wind resource above the building rooftop, as illustrated in Figure 14. These simulations aid in understanding the wind behavior above the building rooftop and identifying zones where flow velocities are below 3 m/s. Such zones will be excluded from the search space during the optimization process.

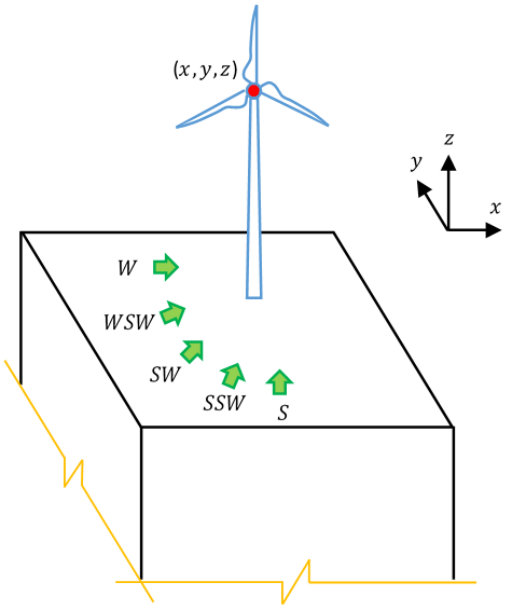

Fig. 14. Representation of wind directions used in the wind resource assessment stage.

The wind velocities obtained in the wind resource assessment are analyzed for different planes, as shown in Figure 15.

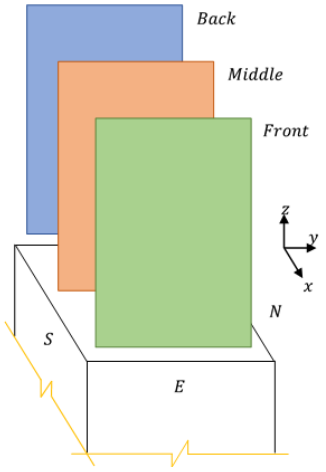

Fig. 15. Planes used to analyze wind speeds.

Figure 16 illustrates the zones where airflow presents velocities lower than 3 m/s (depicted in green) for the middle and back planes above the building rooftop, considering three free wind directions: S, SSW and SW. In Figure 16a, it is evident that the green zone is more extensive in the middle plane compared to the back one. The irregularity of the green zone for SSW and SW is noticeable due to the misalignment with the free airflow, as demonstrated in Figure 16b and Figure 16c.

The wind velocity field obtained in the wind resource assessment will serve as input data for the optimization process. It will be utilized to estimate the amount of wind energy that can be harvested by the wind turbine rotor positioned at specific points above the building rooftop.

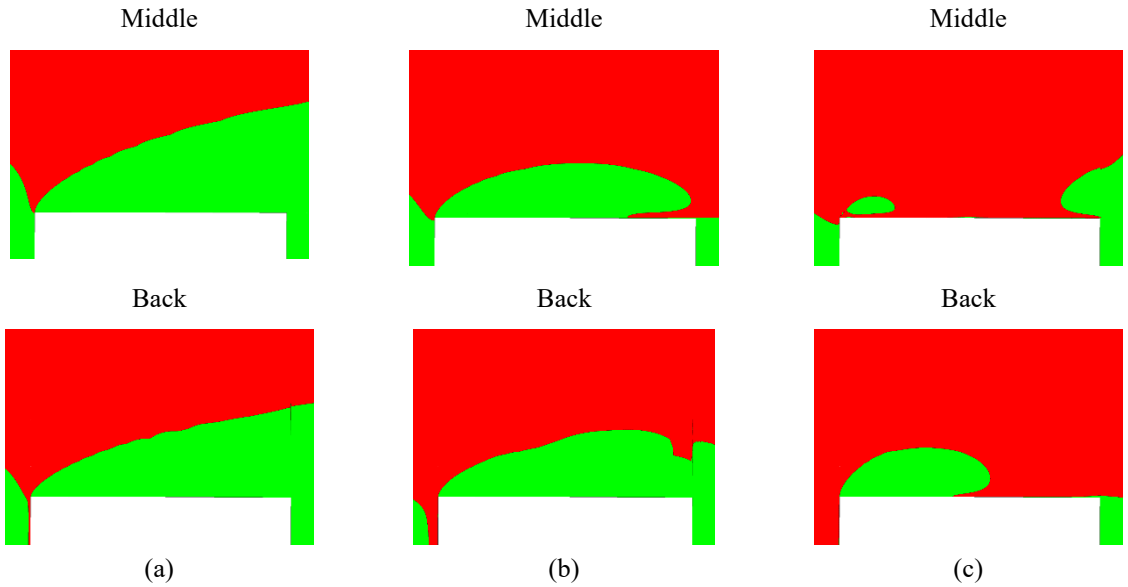

Fig. 16. Wind velocities higher than 3 m/s (red) and lower (green) above the building rooftop for U = 2.44 m/s. Wind directions: S (a), SSW (b) and SW (c).

Figure 17 shows the lower limits, corresponding to different planes as depicted in Figure 15 and Figure 16, above which the wind turbine rotor can be positioned. Zones below these limits are characterized by U below 3 m/s and TI exceeding 20%, respectively. It's worth noting that high turbulence levels can subject wind turbine blades to additional mechanical stress, reducing their operational lifespan [41]. Hence, a lower bound of 37.1 m total height, 7.1 m above the building rooftop, is selected to constrain the search space of the optimization process. Additionally, the upper bound of the search space is constrained by the height of the building above the rooftop, as mentioned in section 3.1.

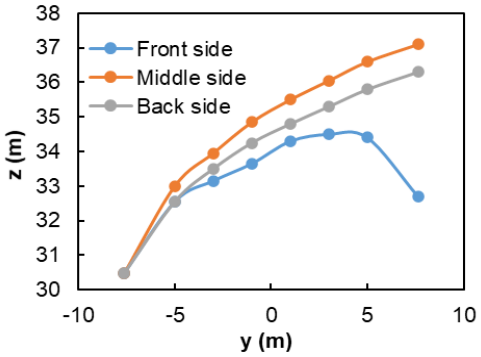

Fig. 17. Lower limits on the building rooftop.

3.5. Wind Turbine Design

The MEXICO wind turbine rotor was utilized in this stage, and CFD simulations were conducted with different wind velocities to estimate its power curve. The estimated power curve is illustrated in Figure 18. Only U lower than 12 m/s were considered in the simulations, as determined in the wind resource assessment stage. Additionally, the power curve calculated here aligns with that derived from experimental measurements in a previous study [42]. The MEXICO wind turbine nearly reaches its design condition, with a nominal rated of 15 kW and a tip speed ratio of 6.67, at U = 15 m/s [27].

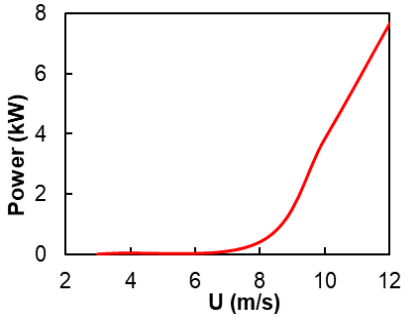

Fig. 18. Power curve of the MEXICO wind turbine.

3.6. Micrositing Optimization

The optimization process depicted in Figure 19 employs a GA to iteratively search for the optimal placement of the wind turbine hub. Initially, GA creates a generation of 30 individuals, where each individual represents a coordinate point (x, y and z) corresponding to a potential wind turbine hub position. A circular area, with a diameter equal to that of the MEXICO wind turbine rotor, is constructed around each coordinate point to extract wind velocities (data obtained from the wind resource assessment stage). These wind velocities are then averaged to compute the wind turbine's power output from the power curve (data from the wind turbine design stage). Additionally, the total yearly energy generated by the turbine is calculated based on the occurrence percentages of wind velocities and directions obtained from the wind rose.

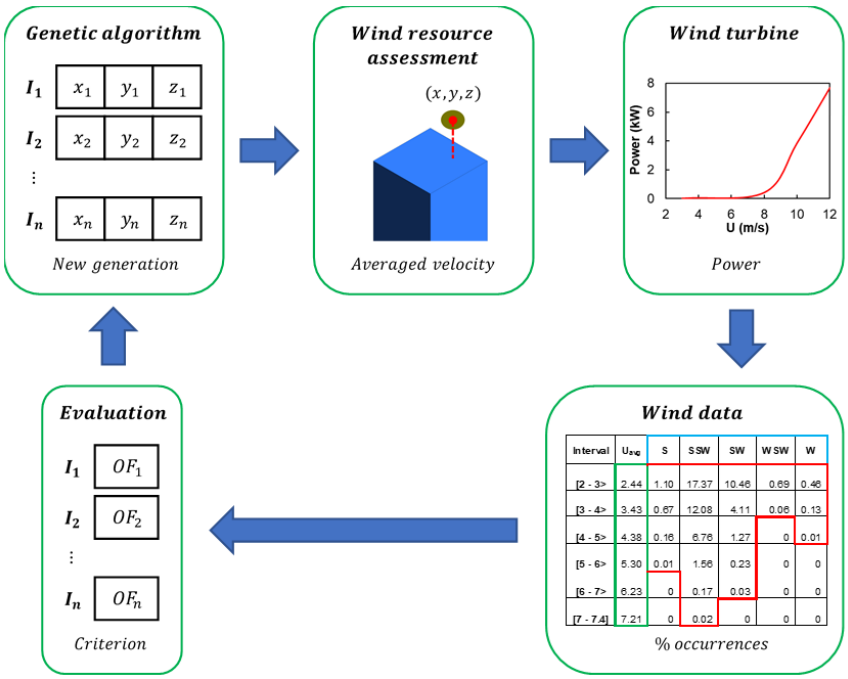

Fig. 19. Flow diagram of the optimization process.

Subsequently, the OF for each individual is evaluated, and the convergence criteria of GA are tested to determine if they are met. If the criteria are not satisfied, GA generates a new generation of 30 individuals to continue the optimization process. Note that this approach requires fewer computational resources compared to simultaneously performing CFD simulations of the building and wind turbine for each generation of GA.

The optimization process results, depicted in Figure 20, illustrate that the algorithm quickly converges to the global optimum by generation 27, achieving a CoE of 3.05146 $/kWh (best) at coordinates 5.322 m, 5.282 m, 60.896 m for x, y and z, respectively. The BMWT generated 1 407.17 kWh/year with a total cost of $ 85 879.

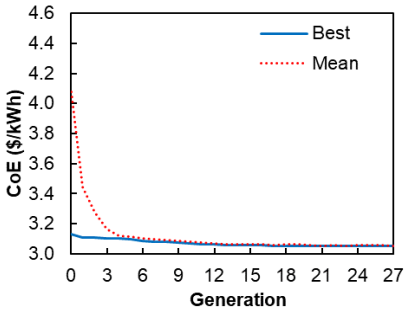

Fig. 20. Objective function of the optimization process.

The best individual is positioned at the upper limit of the search space in the z direction, as shown in Figure 21, where the wind speed is maximum, resulting in the highest energy generation by the BMWT. These results reveal that the yearly energy production by the BMWT is a crucial factor in reducing the CoE. Note that the CoE obtained here appears relatively high compared to other systems [10] [32], primarily due to the mean wind speed (2.3 m/s) in the Jesus Maria district being lower than in previous studies, where it exceeds 4 m/s.

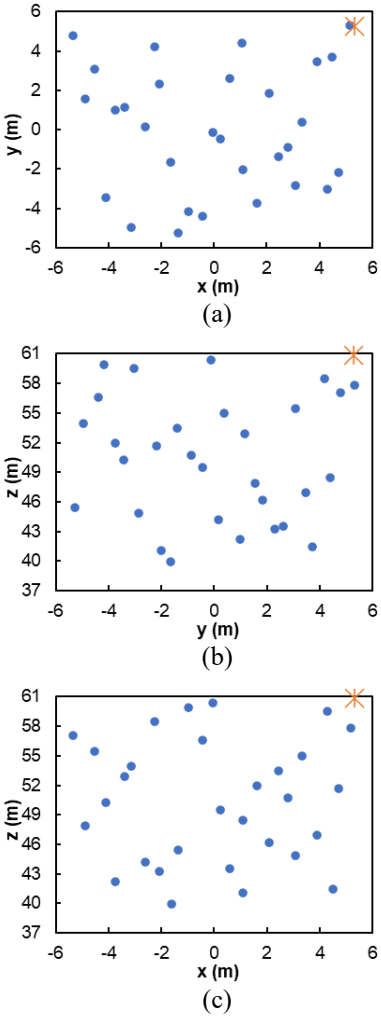

Fig. 21. Position of initial population and best individual. Planes XY (a), YZ (b) and XZ (c).

The sensitivity analysis of the CoE varying F is conducted on the reference plane shown in Figure 22, and the results are presented in Figure 23. In Figure 23a, the lowest CoE of 3.05146 $/kWh (best) is attained for F = 1, situated near the upper limit of the search space in the z direction (blue color), as previously discussed. Similarly, in Figure 23b, for F = 5, the best CoE value is 5.02261 $/kWh. However, as F increases, the position of the lowest CoE decreases in height (z direction), as evident in Figure 23c to Figure 23f, with CoE values of 7.36298 $/kWh, 9.45926 $/kWh, 11.46483 $/kWh and 13.40085 $/kWh, respectively. Note that as F increases, CoE also increases, as expected. Additionally, the lowest CoE is consistently located in the downstream part of the building rooftop across all scenarios. These findings evidence the significant influence of F on CoE, suggesting that F is more important than the total energy generated by the BMWT. It is recommended to conduct further comprehensive analyses regarding the reinforcement costs of buildings where BMWT will be installed; such analyses could be considered as future work.

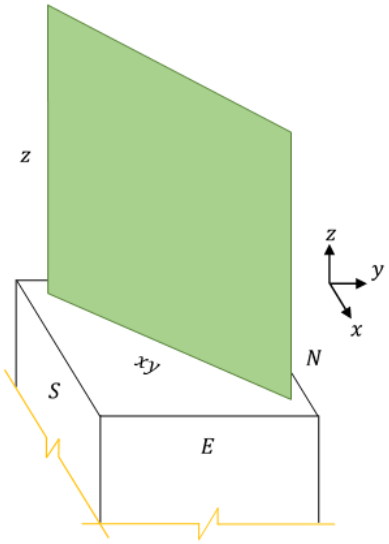

Fig. 22. Plane used in the sensitivity analysis of CoE.

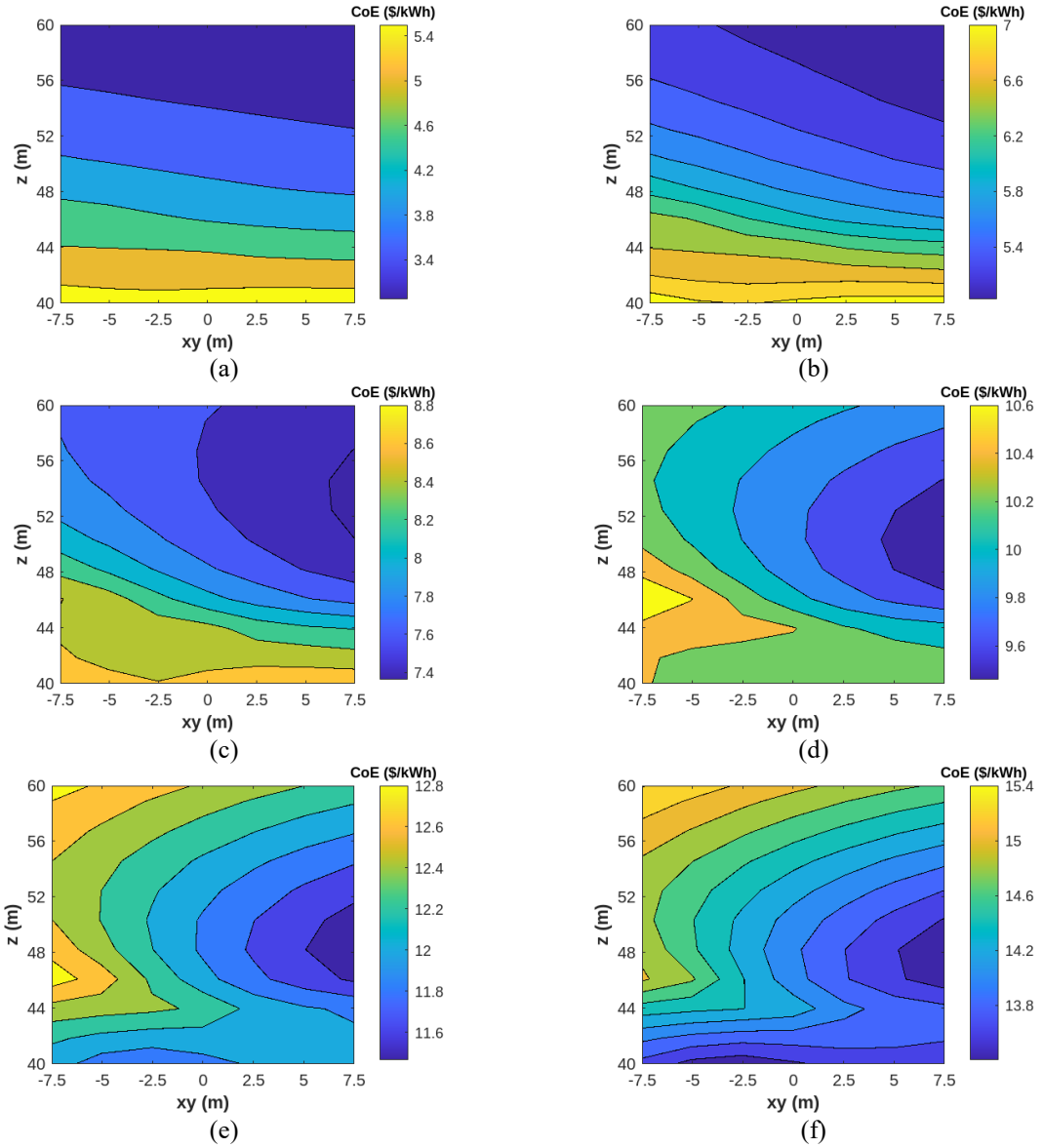

Fig. 23. Sensitivity analysis of CoE for different F values: F = 1 (a), F = 5 (b), F = 10 (c), F = 15 (d), F = 20 (e) and F = 25 (f).

Future work related to the micrositing of BMWTs can include a comprehensive analysis of wind speeds through time-scale modeling [43] [44] [45] and forecasting [46]. Additionally, analyzing different methods for suitably modeling the wind turbine power curve is another issue to be considered [47].

4. Conclusion

The methodology proposed in this work for the optimal micrositing of a BMWT using CFD and GA comprised various key stages aimed at reducing the CoE. Firstly, a site assessment was conducted to evaluate the feasibility of BMWT installation, providing insights and recommendations for the installation. Next, wind data were processed to identify relevant wind velocities and directions necessary for subsequent analysis. CFD simulations were then employed to model wind flow through an urban environment within the wind resource assessment stage. This stage focused in simulating the identified velocities and directions to assess the wind resource above the building rooftop where the BMWT will be installed. The identification of zones with unfavorable wind conditions, characterized by low velocities and high turbulence levels above the building rooftop, played a crucial role in bounding the search space used in the micrositing optimization process. By excluding these areas, the optimization algorithm could focus on finding the optimal position for the BMWT that maximized energy production while minimized installation costs. Moreover, the comparison of simulation results with experimental measurements during the validation stage ensured the reliability and accuracy of the computational models used for both the urban environment and the wind turbine. Furthermore, the simulation of the wind turbine was essential for computing its power curve, which served for estimating its energy production under different wind conditions. A simplified cost model was used for determining the total cost of installation, while the estimation of energy production by the BMWT relied on wind data predicted in the wind resource assessment stage and the power curve of the turbine. Additionally, the sensitivity analysis conducted to assess the influence F on the CoE enhanced the understanding of how variations in certain parameters could impact the overall economics of the wind system.

The methodology presented in this work offers several advantages compared to previous studies in the field of micrositing for BMWTs. One advantage is the inclusion of an initial site assessment, which helps evaluate the feasibility and suitability of installing BMWTs in a specific urban environment. Furthermore, the wind resource assessment stage in this methodology, unlike past studies that often simulated only one wind velocity and direction, considers multiple wind velocities and directions, reflecting the multidirectional behavior of on-site wind conditions accurately. Another advantage is the incorporation of the micrositing optimization into the methodology. By using GA and CFD simulations, the proposed approach allows for the optimization of BMWT placement to maximize power output and minimize CoE. Additionally, the methodology facilitates the analysis of multiple BMWT placements by decoupling CFD simulations of the building and wind turbine. By optimizing multiple turbine placements simultaneously, the methodology offers flexibility for evaluating different installation scenarios.

The site selected for this study was a hypothetical building. During the site assessment, only one restriction was considered regarding the visual impact of wind turbine blades on humans, bounding the lower limit of available space. Additionally, the upper limit of available space was bounded by the height of the building above the rooftop. Wind data used in the analysis was sourced from the Campo de Marte station in the Jesus Maria district (Lima, Peru), covering measurements from January 1st to December 31st of 2020. Analysis of the wind data revealed that the majority of daily average wind velocities fell within the range of 1.5 to 3 m/s, with an average yearly wind velocity of 2.3 m/s. Furthermore, a significant amount of these velocities occurred in the SSW and SW directions, accumulating 81.8% of occurrences. Additionally, wind velocities ranging from S to W directions accounted for 94.7% of the total occurrences.

Since most wind turbines have a cut-in speed above 3 m/s, it was unnecessary to simulate wind velocities below this threshold. Consequently, while 20 cases were considered in the wind resource assessment stage, only 15 cases were simulated, specifically those corresponding to wind directions of S, SSW, and SW. This decision was influenced by the symmetry of the building topology, which allowed for the exclusion of certain wind directions from the CFD simulations.

The grid independence study of the building results revealed minimal discrepancies between the Medium and Fine meshes, with deviations for U not exceeding 1.35% and negligible differences in k. Consequently, the Medium mesh, consisting of 8,101,184 cells, was selected for subsequent simulations. To comply with the requirement of avoiding zones with $U < 3$ m/s and $TI > 20\%$, a lower bound of 37.1 m total height (7.1 m above the building rooftop) was established for the search space in the GA-based optimization process.

The validation of the MEXICO wind turbine results, conducted in a prior study, confirmed that the mesh independence was achieved with the Medium mesh (8,094,168 cells), since deviations between the numerical results of the Medium and Fine meshes remained below 0.8% and 2.2% for thrust and torque, respectively. Hence, the Medium mesh was used for simulations of subsequent stages.

On the other hand, to construct the turbine power curve, only wind velocities less than 12 m/s were considered. This wind velocity represents the upper limit achieved in the study area, as determined in the wind resource assessment stage.

In the optimization process, the population consisted of 30 individuals representing coordinate points (x, y and z) corresponding to hub positions of the MEXICO wind turbine. GA converged at generation 27, achieving a CoE of 3.05146 $/kWh (best) at coordinates 5.322 m, 5.282 m, 60.896 m (x, y and z). The wind turbine generated 1,407.17 kWh/year with a total cost of $85,879. This highlights the significance of yearly energy production in reducing the CoE. The relatively high CoE obtained in this study compared to past works can be attributed to the low average wind speed in the Jesus Maria

district (2.3 m/s). Moreover, the sensitivity analysis of CoE varying f demonstrated that as F increases, the position of the lowest CoE shifts downwards in the z direction. For F values of 1 and 25, CoE of 3.05146 and 13.40085 $/kWh were obtained, respectively. This underscores the increasing importance of F in reducing the CoE of the BMWT as its value rises.

Acknowledgements

Christian V. Rodriguez is thankful to Concejo Nacional de Ciencia, Tecnología e Innovación (CONCYTEC) for granting the fellowship that made possible the development of this paper. Christian Rodriguez also thanks to Servicio Nacional de Meteorología e Hidrología (SENAMHI) for providing the data of Jesús María monitoring station.

Author Contributions

Christian V. Rodriguez contributed to the development of the methodology, conducted the formal analysis, developed the software, and prepared the original draft of the manuscript. Alberto Ríos led the conceptualization and supervision of the study and participated in the review and editing of the manuscript. Jaime E. Luyo was involved in the review and editing process. All authors have read and approved the final version of the manuscript.

Conflict of Interest

The authors declare that they have no known competing financial interests or personal relationships that could have appeared to influence the work reported in this paper.

References

[1] E. Arteaga-López, C. Ángeles-Camacho, and F. Bañuelos-Ruedas, "Advanced methodology for feasibility studies on building-mounted wind turbines installation in urban environment: Applying CFD analysis," Energy, vol. 167, pp. 181–188, 2019. doi: 10.1016/j.energy.2018.10.191.

[2] IEC, "IEC 61400-2:2013 – Wind turbines – Part 2: Small wind turbines," 2013.

[3] S. P. Evans, A. K. C., D. R. Bradney, T. P. Urmee, J. Whale, and P. D. Clausen, "The suitability of the IEC 61400-2 wind model for small wind turbines operating in the built environment," Renewable Energy and Environmental Sustainability, vol. 2, p. 31, 2017. doi: 10.1051/rees/2017022.

[4] M. I. Rakib, S. Nay, S. Evans, and P. Clausen, "Wind regimes in urban environments: Experimental comparison with the IEC 61400-2:2013 open terrain wind model," in Research Topics in Wind Energy, vol. 8, pp. 201–214, 2019. doi: 10.1007/978-3-030-13531-7_12.

[5] M. Ghasemian, Z. N. Ashrafi, and A. Sedaghat, "A review on computational fluid dynamic simulation techniques for Darrieus vertical axis wind turbines," Energy Conversion and Management, vol. 149, pp. 87–100, 2017. doi: 10.1016/j.enconman.2017.07.016.

[6] M. A. Heath, J. D. Walshe, and S. J. Watson, "Estimating the potential yield of small building-mounted wind turbines," Wind Energy, vol. 10, no. 3, pp. 271–287, 2007. doi: 10.1002/we.222.

[7] A. B. Tabrizi, J. Whale, T. Lyons, and T. Urmee, "Performance and safety of rooftop wind turbines: Use of CFD to gain insight into inflow conditions," Renewable Energy, vol. 67, pp. 242–251, 2014. doi: 10.1016/j.renene.2013.11.033.

[8] Y. H. Juan, C. Y. Wen, W. Y. Chen, and A. S. Yang, "Numerical assessments of wind power potential and installation arrangements in realistic highly urbanized areas," Renewable and Sustainable Energy Reviews, vol. 135, p. 110165, 2021. doi: 10.1016/j.rser.2020.110165.

[9] A. Gagliano, F. Nocera, F. Patania, and A. Capizzi, "Assessment of micro-wind turbines performance in urban environments," International Journal of Energy and Environmental Engineering, vol. 4, no. 1, pp. 1–14, 2013. doi: 10.1186/2251-6832-4-43.

[10] Q. Deltenre and M. C. Runacres, "Installation of a small building-mounted wind turbine: A case study from idea to implementation," in Research Topics in Wind Energy, vol. 8, pp. 71–88, 2019. doi: 10.1007/978-3-030-13531-7_5.

[11] M. Z. Shiraz, A. Dilimulati, and M. Paraschivoiu, "Wind power potential assessment of roof-mounted wind turbines in cities," Sustainable Cities and Society, vol. 53, 2020. doi: 10.1016/j.scs.2019.101905.

[12] K. Chen, M. X. Song, X. Zhang, and S. F. Wang, "Wind turbine layout optimization with multiple hub height wind turbines using greedy algorithm," Renewable Energy, vol. 96, pp. 676–686, 2016. doi: 10.1016/j.renene.2016.05.018.

[13] C. B. Moorthy, M. K. Deshmukh, and D. Mukherejee, "New approach for placing wind turbines in a wind farm using genetic algorithm," Wind Engineering, vol. 38, no. 6, pp. 633–642, 2014.

[14] C. B. Moorthy and M. K. Deshmukh, "A new approach to optimise placement of wind turbines using particle swarm optimisation," International Journal of Sustainable Energy, vol. 34, no. 6, pp. 396–405, 2015. doi: 10.1080/14786451.2013.860140.

[15] S. Rajper and I. J. Amin, "Optimization of wind turbine micrositing: A comparative study," Renewable and Sustainable Energy Reviews, vol. 16, no. 8, pp. 5485–5492, 2012. doi: 10.1016/j.rser.2012.06.014.

[16] M. X. Song, K. Chen, and J. Wang, "Three-dimensional wind turbine positioning using Gaussian particle swarm optimization with differential evolution," Journal of Wind Engineering and Industrial Aerodynamics, vol. 172, pp. 317–324, 2018. doi: 10.1016/j.jweia.2017.10.032.

[17] W. Hu, Q. Yang, H.P. Chen, K. Guo, T. Zhou, M. Liu, J. Zhang, Z. Yuan, "A novel approach for wind farm micro-siting in complex terrain based on an improved genetic algorithm," Energy, vol. 251, 2022. doi: 10.1016/j.energy.2022.123970.

[18] B. Ovgor, S. K. Lee, and S. Lee, "Micrositing of wind turbine on building rooftop using CFD and wind distribution," Journal of Mechanical Science and Technology, vol. 26, no. 12, pp. 3981–3988, 2012. doi: 10.1007/s12206-012-0897-2.

[19] Q. Wang, J. Wang, Y. Hou, R. Yuan, K. Luo, and J. Fan, "Micrositing of roof-mounted wind turbines in urban environment," Renewable Energy, vol. 115, pp. 1118–1133, 2018. doi: 10.1016/j.renene.2017.09.045.

[20] E. Arteaga-López and C. Ángeles-Camacho, "Innovative virtual computational domain based on wind rose diagrams for micrositing small wind turbines," Energy, vol. 220, 2021. doi: 10.1016/j.energy.2020.119701.

[21] C. C. Moreira Chagas, M. G. Pereira, L. P. Rosa, N. F. da Silva, M. A. V. Freitas, and J. D. Hunt, "From megawatts to kilowatts: A review of small wind turbine applications," Sustainability, vol. 12, no. 7, p. 2760, 2020. doi: 10.3390/su12072760.

[22] "Windrose," GitHub repository. [Online]. Available: https://github.com/python-windrose/windrose

[23] C. V. Rodriguez, A. Ríos, and J. E. Luyo, "High-rise building and horizontal axis wind turbine CFD models validation using two RANS turbulence models," International Journal of Renewable Energy Research, vol. 16, no. 2, 2026.

[24] T.-H. Shih, W. W. Liou, A. Shabbir, Z. Yang, and J. Zhu, "A new k-ε eddy viscosity model for high Reynolds number turbulent flows," Computers & Fluids, vol. 24, no. 3, pp. 227–238, 1995. doi: 10.1016/0045-7930(94)00032-T.

[25] J. G. Schepers and H. Snel, Model Experiments in Controlled Conditions, 2007.

[26] F. R. Menter, "Two-equation eddy-viscosity turbulence models for engineering applications," AIAA Journal, vol. 32, no. 8, pp. 1598–1605, 1994. doi: 10.2514/3.12149.

[27] H. Snel, J. G. Schepers, and N. B. Siccama, "Mexico project: Database and results," AIAA Aerospace Sciences Meeting, 2009. doi: 10.2514/6.2009-1217.

[28] National Renewable Energy Laboratory, Wind Resource Assessment Handbook, 1997.

[29] J. F. Manwell, J. G. McGowan, and A. L. Rogers, Wind Energy Explained: Theory, Design and Application, 2010. doi: 10.1002/9781119994367.

[30] L. Fingersh, M. Hand, and A. Laxson, "Wind turbine design cost and scaling model," NREL, 2006.

[31] A. Rezaeiha, H. Montazeri, and B. Blocken, "Framework for large-scale urban wind energy assessment," Energy Conversion and Management, vol. 214, p. 112770, 2020. doi: 10.1016/j.enconman.2020.112770.

[32] T. Stehly, P. Beiter, and P. Duffy, "2019 cost of wind energy review," NREL, 2019.

[33] A. C. Orrell and H. E. Rhoads, "2013 distributed wind market report," 2013.

[34] A. C. Orrell and N. F. Foster, "2014 distributed wind market report," 2014.

[35] A. Hassanat, K. Almohammadi, E. Alkafaween, E. Abunawas, A. Hammouri, and V. B. S. Prasath, "Choosing mutation and crossover ratios for genetic algorithms," Information, vol. 10, no. 12, 2019. doi: 10.3390/info10120390.

[36] Z. Michalewicz and M. Schoenauer, "Evolutionary algorithms for constrained parameter optimization problems."

[37] S. Katoch, S. S. Chauhan, and V. Kumar, "A review on genetic algorithm," Multimedia Tools and Applications, vol. 80, no. 5, pp. 8091–8126, 2021. doi: 10.1007/s11042-020-10139-6.

[38] N. Dey, Applied Genetic Algorithm and Its Variants, 2023.

[39] N. M. Razali and J. Geraghty, "Genetic algorithm performance with different selection strategies," World Congress on Engineering, 2011.

[40] C. V. Rodriguez and C. Celis, "Design optimization methodology of small wind turbine blades," Journal of the Brazilian Society of Mechanical Sciences and Engineering, vol. 44, no. 6, p. 254, 2022.

[41] M. De Prada Gil, O. Gomis-Bellmunt, A. Sumper, and J. Bergas-Jané, "Power generation efficiency analysis of offshore wind farms," Energy, vol. 37, no. 1, pp. 455–468, 2012.

[42] X. Wang, W. Z. Shen, J. Z. Wei, N. S. Jens, and J. Chen, "Shape optimization of wind turbine blades," Wind Energy, vol. 12, no. 8, pp. 781–803, 2009.

[43] I. Colak, S. Sagiroglu, M. Yesilbudak, E. Kabalci, and I. Bulbul, "Wind speed and power forecasting," ICRERA, Palermo, Italy, 2015.

[44] O. Kaplan and M. Temiz, "Wind speed potential analysis in Ankara," ICRERA, Birmingham, UK, 2016.

[45] S. Basile, R. Burlon, and F. Morales, "Joint probability distributions for wind speed and direction," ICRERA, Palermo, Italy, 2015.

[46] A. R. Finamore, V. Calderaro, V. Galdi, A. Piccolo, G. Conio, and S. Grasso, "Day-ahead wind speed forecasting using neural networks," ICRERA, Palermo, Italy, 2015.

[47] R. J. De Andrade Vieira and M. A. Sanz-Bobi, "Power curve modelling of wind turbines," ICRERA, Palermo, Italy, 2015.